Measurement of Amorphous Orientation in Poly(ethylene terephthalate) Fibers by X-Ray Diffraction and Its Significance

N. S. MURTHY,[1] C. BEDNARCZYK,[1] P. B. RIM,[2] C. J. NELSON[2]

[1] Research and Technology, AlliedSignal Inc., P. O. Box 1021, Morristown, New Jersey 07962

[2] Fibers Division Technical Center, AlliedSignal Inc., Petersburg, Virginia 23804

Received 12 September 1996; accepted 29 October 1996

ABSTRACT: The orientation of the noncrystalline (amorphous) phase in poly (ethylene terephthalate) fibers is analyzed by separating the amorphous scattering in the wide-angle x-ray diffraction patterns into isotropic and anisotropic components. Two parameters are used to characterize the amorphous orientation—the fraction of the anisotropic component and its degree of orientation. The x-ray amorphous orientation parameters are compared with the sonic modulus and the birefringence values. Our results illustrate that the intrinsic birefringence of the amorphous phase is not "intrinsic" but depends on its density. The role of the oriented amorphous phase in determining the strength (tenacity) and the dimensional stability (shrinkage) of the fibers is discussed. We conclude that although amorphous orientation determines the shrinkage, other factors such as the connectivity between the amorphous phase and the crystalline regions play an important role in determining the tenacity of the fibers. © 1997 John Wiley & Sons, Inc. J Appl Polym Sci **64:** 1363–1371, 1997

INTRODUCTION

Poly(ethylene terephthalate), PET, is generally considered as a two phase system consisting of crystalline lamellae and the noncrystalline segments outside the lamellae. The noncrystalline phase has been traditionally referred to as the amorphous phase, although it is commonly understood that the amorphous chain segments outside the lamellae can have some local order. The extent of the short-or medium-range order within the amorphous phase, the density, orientation, and the conformation of the amorphous chain segments greatly influence the performance of a polymer. In the particular case of fibers, mechanical properties such as modulus and tenacity, and diffusion behavior such as dye uptake and permeability, are influenced by the amorphous orientation. Among the techniques available for determining the amorphous orientation, optical birefringence, sonic modulus, and spectroscopic (dichroic ratio) measurements are the most widely used (see ref. 1). These techniques probe different aspects of the amorphous domains. Optical birefringence values depend on the differences in the polarizability (refractive indices) of the oriented domains along and perpendicular to the fiber axis. The sonic modulus results depend on the variations in the velocity of the sound waves with the orientation of the amorphous regions. Both these techniques require a knowledge of the crystallinity of the polymer,

Correspondence to: N. S. Murthy.

whereas the value of the transition moment angle needs to be known for the dichroic ratio measurements. Each of these techniques have some inherent limitations. For instance, the amorphous orientation calculated from the crystallinity and the birefringence data might be ambiguous if correct values of the intrinsic birefringence of the crystalline and the amorphous domains are not known. Similarly, a knowledge of the modulus of the crystalline and amorphous regions are necessary for using the sonic modulus methods. Because it is known that the amorphous density could vary with orientation, the amorphous birefringence and the amorphous modulus are also likely to vary with orientation.

Because of these uncertainties in the commonly used techniques, we have investigated the utility of the x-ray diffraction (XRD) methods to evaluate amorphous orientation.[2–6] It so happens that to completely describe the amorphous halo, one has to separate the amorphous scattering into unoriented and oriented components. The idea that the amorphous phase can be separated into two components has been discussed previously in the literature. Most notable is the work of Jellinnek for PET.[2] Harget and Oswald later used this approach to quantitatively evaluate the degree of orientation of the oriented component and the fraction of the oriented component in amorphous PET fibers.[3] Recently, Urbanczyk carried out a similar analysis on PET and N6 fibers.[4] We independently rediscovered the importance of separating the amorphous phase into two components, and have applied it nylon 6[5] and PET.[6] Further, we have improved the precision of such measurements by taking into account the influence of the structure in the amorphous phase on the shape of the amorphous halo.

In this article we illustrate the x-ray method using the data from high-modulus, low-shrinkage (HMLS) PET fibers produced without any thermal treatment subsequent to drawing. We compare these values with optical birefringence and sonic modulus data, and discuss how amorphous orientation influences the tenacity and the shrinkage behavior of these fibers. We also show that the radial intensity variations at various azimuthal angles used in these analyses provide us with a unique perspective of the structure and the orientation of the amorphous phase in semicrystalline polymers. We will discuss the implications of our measurements of the amorphous characteristics on the properties (strength and dimensional stability) of the fibers.

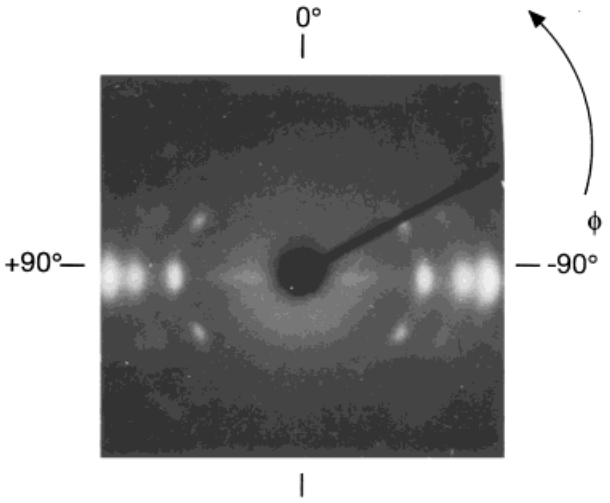

Figure 1 X-ray diffraction photograph of a PET fiber to illustrate our data collection scheme.

MATERIALS AND METHODS

Three PET fibers made by AlliedSignal were analyzed: 1W70, 1W90, and A330. 1W70 and 1W90 are high-modulus and high-tenacity fibers, and A330 is experimental version the recently introduced dimensionally stable fiber 1×30. Some of the properties of these fibers have been described in an article by Rim and Nelson.[7] An undrawn, amorphous precursor to 1W90 was also included in the analysis.

Wide-angle radial XRD scans were obtained on a Philips vertical goniometer APD-3600 in the symmetrical transmission mode ($\theta/2\theta$) using CuKα radiation. The incident and receiving slits for the x-ray beam were 1/2° and 1°, respectively. The scattering data were collected from 2θ = 10–35° in 0.1° steps for a period of 10 s per step. The fiber sample was wound around a small brass toothed holder so that the fibers are held parallel to each other. A series of radial scans were obtained at various azimuthal angles ϕ by rotating the fiber in its own plane (Fig. 1) between ϕ = −90° to 90° in steps ranging from 5–15°. About 20–25 radial scans were obtained from 1W70, 1W90, and A330 fibers, and about eight scans from ϕ = 0° to 90° for the 1W90-precursor fiber.

The data were analyzed using a modified version of the program SHADOW.[8,9] The background

was determined using a linear fit for the first and the last few data points (2θ = 5° and 35°). The crystalline and amorphous peaks were then fitted with modified Lorentzian profiles. The scans near the equator ($\phi = 0 \pm 15°$) were fitted with three or four crystalline peaks and two amorphous halos; the position of the amorphous halos were restricted to $2\theta = 17.5 \pm 1°$ and $23.0 \pm 1°$, but the height and full-width at half maximum (FWHM) were allowed to vary. The scans near the meridian (ϕ = 90° and $-90 \pm 15°$) were fitted with two crystalline peaks and two amorphous halos ($\sim$ 16.3 and 22.1° The shift in the position of the amorphous halo to lower angles in going from equator to the meridian noted here in PET fibers has been observed in other polymers as well, for example in nylon 6,[5] and polyethylene[10] (see the Results section for further elaboration). Scans between the equatorial and meridional regions were also fitted with two to three crystalline peaks and two amorphous halos; the position, FWHM, and intensity of the two amorphous halos were not fixed. No crystalline peaks were used in fitting the data from the amorphous fiber.

The variation in height of the amorphous halo at 2θ = 23° was plotted as a function of azimuthal angle, ϕ. This second peak could be evaluated more precisely than the first peak at 2θ = 17.5°. This I(ϕ) plot was fitted with Gaussian peak and a linear baseline. The FWHM of such I(ϕ) curves was used to calculate the degree of orientation, f_a. The peak area normalized to the total area under the I(ϕ) curve was used to obtain the oriented amorphous fraction F_a.

RESULTS

A representative series of radial scans at various azimuthal angles are shown in Figure 2 to illustrate the key features of the XRD scans in oriented PET. In all the samples, the position of the amorphous halo at 2θ = 23° shifts to a higher angle in going from the meridian towards the equator ($2\theta \sim 21°$ near the meridian and $\sim$ 23° near the equator); this is accompanied by a decrease in the width of the amorphous peaks. These changes in the position and FWHM of this halo signify that the amorphous chain segments oriented parallel to the fiber axis are more densely packed than those that are either randomly oriented or oriented perpendicular to the fiber axis. Some examples of the profile analyses are shown

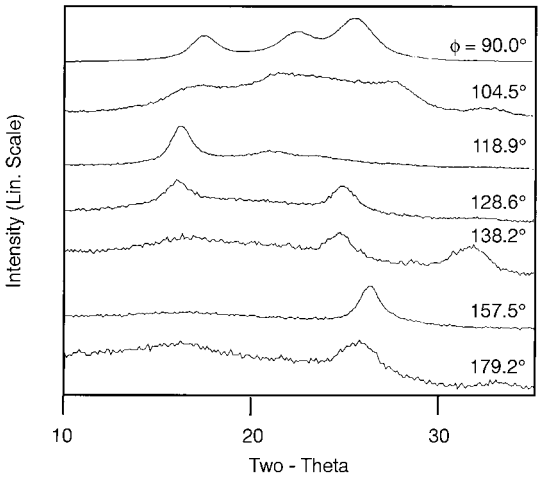

Figure 2 Radial (symmetrical transmission) scans of a drawn PET fiber at the azimuthal angles indicated next to each of the curves.

in Figure 3. The intensity of the amorphous halo at $2\theta \sim 23°$ is plotted as a function of the azimuthal angle (Fig. 4) to determine the amorphous orientation. Such plots for the crystalline peaks have zero baselines, whereas those for the amorphous peaks rarely have zero baselines. This immediately suggests that at least two parameters are required to describe such amorphous intensity vs. ϕ plots; one takes into account the height of the baseline and the other the width of the peak. We attribute the area under the baseline to the unoriented amorphous component, and the area within the peak to the oriented component.

Figure 5 shows the variations in the distribution of the intensity in the amorphous halo upon drawing a fiber (the undrawn fiber is amorphous and the drawn fiber is semicrystalline). The most noticeable effect of drawing on these XRD plots is the drop in the baseline and the narrowing of the peak. Thus, the effect of drawing is to decrease the unoriented fraction and increase the degree of orientation of the oriented fraction. We use two parameters, f_a and F_a to describe the changes in the amorphous phase. f_a is the Hermans orientation function calculated from the width of the peak and F_a is the ratio $A_p/(A_p + A_b)$, in which A_p is the area of the peak and A_b is the area under the baseline; A_b = height of the baseline $\times$ 180. F_a represents the fraction of the anisotropic phase, and f_a represents the orientation of the anisotropic phase. A single Hermans orientation function $\langle f_a \rangle$ can also be calculated from the relation

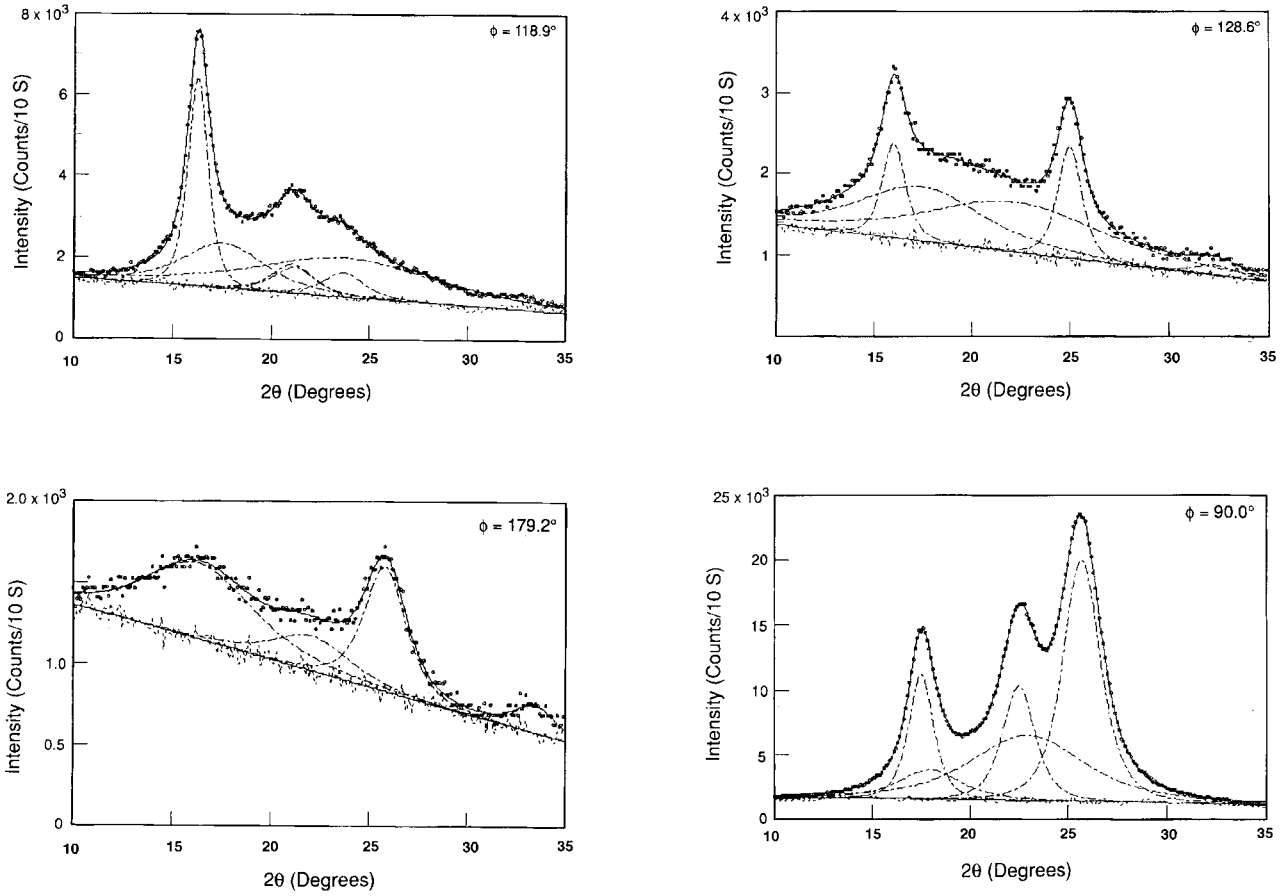

Figure 3 Profile analysis of four representative scans. The observed data points are shown by circles. The observed scan is resolved into various components, which are shown by the dashed lines. The full line through the observed data is the sum of the resolved component peaks. The baseline is also shown as full line. The dashed line near the baseline is the difference between the observed intensities and the fitted values.

$$\langle f_a \rangle = (3 \langle \cos^2\phi \rangle - 1)/2;$$

$$\langle \cos^2\phi \rangle = \int_0^{\pi} \mathrm{I}(\phi)\cos^2\phi \sin\phi d\phi \Big/ \int_0^{\pi} \mathrm{I}(\phi)\sin\phi \, d\phi$$

in which $\mathrm{I}(\phi)$ is the total height of the amorphous scattering at ϕ. However, $\langle f_a \rangle$ is less sensitive to the variations in the height of the baseline than F_a. The f_a and the F_a values for the various fibers are tabulated in Table I. The most significant difference in the amorphous scattering of these samples is that both f_a and F_a of the fibers vary in the following sequence: A330 > 1W90 > 1W70.

DISCUSSION

An obvious feature in the azimuthal intensity distributions of the amorphous scattering in all polymers is the nonzero baseline (Fig. 4).[1–5,11] This nonzero baseline, which represents isotropic or unoriented amorphous scattering, is present even in highly drawn fibers. In contrast, the crystalline peaks show little or no unoriented component, i.e., baseline is almost invariably zero. Exceptions are the poorly oriented semicrystalline polymers, and polymers that have been annealed after drawing. The separation of the amorphous scattering into two components, areas below and above the baseline, may not be just an analytical tool to interpret the data, but could be due to the presence of iso-

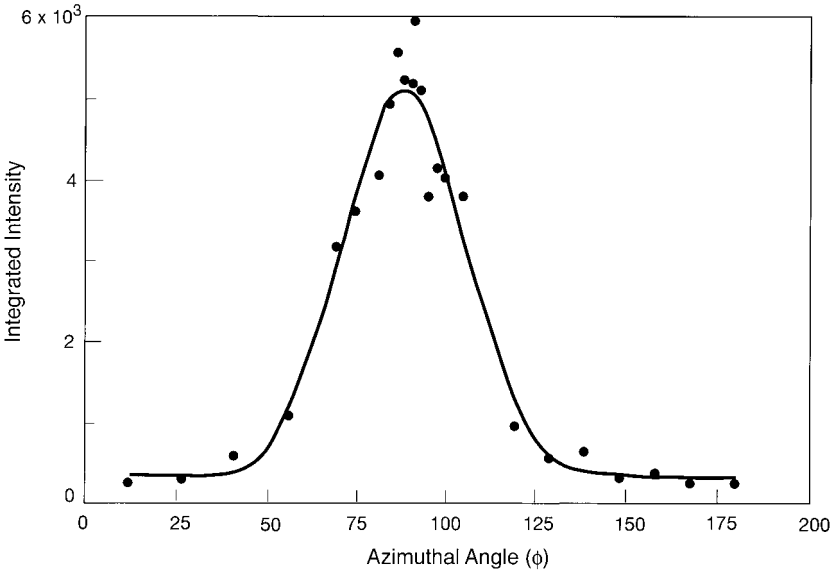

Figure 4 Plot of the amorphous intensities (peak heights of the halo at 23°) as a function of the azimuthal angle.

tropic and anisotropic components in the amorphous regions. For instance, the oriented fraction might correspond to the interfibrillar regions, and the unoriented fraction to the amorphous phase within a fibril. It is also expected that the influence of the unoriented and oriented amorphous regions on the mechanical behavior of the material will be different.

In analyzing the azimuthal intensity distribution of the amorphous halo, we have assigned the area above the baseline to anisotropic component and the area below the baseline to the isotropic component of a single amorphous phase. Recall that the area above the baseline is concentrated around the equator and the area below the baseline is determined by the meridional amorphous scattering. Wunderlich and co-workers assume that the amorphous phase should be unoriented, and any oriented diffuse scattering should be attributed to an intermediate phase distinct from the crystalline and the amorphous phases.[12,13] But, for the same reason that oriented rubbery phase in a drawn amorphous polymer is not a new phase, the oriented amorphous phase is not necessarily a distinct third phase. The characteristics of the amorphous phase could vary continuously with the degree of orientation. The question whether the intensity above the baseline in Figure 4 is due to a new intermediate phase or if the whole scattering is from a single amorphous phase, is somewhat analogous to the question whether the diffuse scattering in the diffraction pattern of a semicrystalline polymer is due to an amorphous phase, or to the defects in the crystalline domains.[14,15] Because even semicrystalline polymers exhibit a glass transition temperature, the diffuse scattering is indeed due to a distinct amorphous phase. Because the meridional and equatorial amorphous scattering are only quantitatively different, and because the anisotropic component behaves like an amorphous phase in the sense that it exhibits glass transition behavior, we will regard the anisotropic and the isotropic amorphous "phases" as two components of a single noncrystalline or amorphous phase.

The orientation of the amorphous phase as measured here by the XRD methods refer to the orientation of the noncrystalline domains of size $\sim$ 30 Å. Sonic modulus and optical birefringence (excluding form birefringence) depend on dipole orientation and molecular deformation, respectively, and hence, measure the anisotropy on a molecular scale. Our values of the amorphous orientation related to the oriented amorphous component, f_a and F_a, correlate well with the birefringence and sonic modulus data in drawn fibers (Fig. 6). The average amorphous orientation, $\langle f_a \rangle$, calculated from the whole amorphous intensity, agrees well with the value calculated from birefringence measurement only for the amorphous precursor fiber (Table I). In the semicrystalline fibers, the birefringence values tend to

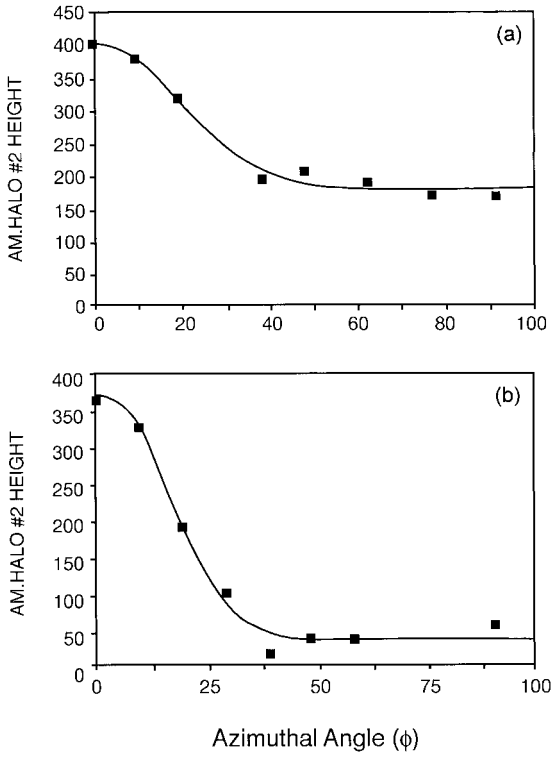

Figure 5 Comparison of the amorphous intensity variations in the amorphous halo at $2\theta = 23°$ in (a) undrawn and (b) drawn fiber.

agree with f_a (from the peak width) and not with $\langle f_a \rangle$. This implies that the intrinsic birefringence values used in the calculation of f_a (optical) refers only to the anisotropic phase and not to the whole amorphous phase. A some what similar situation was found in the analysis of nylon 6 fibers as well.[16] Such discrepancies between the optical and the x-ray values may not be surprising in view of the controversy surrounding the value for intrinsic amorphous birefringence.[17–19]

Harget and Oswald using the two-phase model, and assuming that the amorphous phase could be separated into oriented and unoriented components, calculated the anisotropic component of the amorphous halo and the degree of amorphous orientation.[3] Additionally, they obtained a value of 0.410 for the intrinsic birefringence of the oriented amorphous phase, Δ_a^o. Biangardi, in a commentary on Harget and Oswald's article showed that Δ_a^o is indeed 0.2688.[20] By analyzing the data from the amorphous precursor to the 1W90 fiber (Table I), we have found that this discrepancy is because Harget and Oswald calculate the orientation of only the anisotropic component, whereas both anisotropic and isotropic components are used in the calculations of Biangardi. Thus, the value of 0.410 obtained is "intrinsic" to the oriented amorphous component, and the "intrinsic" birefringence of the combined unoriented and oriented components will obviously be less than 0.410.

In calculating the amorphous orientation (optical) in Table I, we have used the most often cited intrinsic birefringence values of 0.220 and 0.275 for the crystalline (Δ_c^o) and amorphous (Δ_a^o) fractions, respectively.[17] The value for Δ_a^o used here has been independently reproduced by some,[18,19] and disputed by others.[21,22] The calculation of Δ_a^o requires a knowledge of the crystallinity of the sample. Very often these crystallinities are calculated from density measurements assuming constant amorphous density, which introduces some uncertainties in the reported values of Δ_a^o because the amorphous density is not necessarily constant.[6] Also, Δ_c^o and Δ_a^o are expected to depend

Table I[a] Comparison of Structural Parameters and the Fiber Properties in PET Fibers

	Fiber			
Parameter	1W90U	1W70	1W90	A330
Shrinkage (%)[b]		12.5	9.6	7.5
Ultimate Elongation (%)		13.7	11.1	10.5
LASE-5 (g/day)[c]		3.62	3.67	4.14
Tenacity (g/day)		9.2	8.1	7.9
Sonic Modulus (g/day)		195	168	164
T_m		256.1	257.5	259.1
L (Å)		136	113	106
density (g/cc)		1.3898	1.3857	1.3864
Crystallinity by density		37	34	35
XRD CI (%)	0.0	35	37	38
Δn	0.026	0.2322	0.2026	0.1972
f_c (XRD)		0.96	0.96	0.96
f_a (Optical)	0.095	0.88	0.71	0.68
$\langle f_a \rangle$ (XRD)	0.082	0.423	0.342	0.301
f_a (XRD)[d]	0.733	0.776	0.729	0.671
F_a (XRD)	0.389	0.771	0.691	0.648

[a] Some of the data are from ref. 7.
[b] At 177°C and 9 g tension.
[c] Load at a specified elongation of 5%.
[d] Form the peak at $2\theta = 23°$.

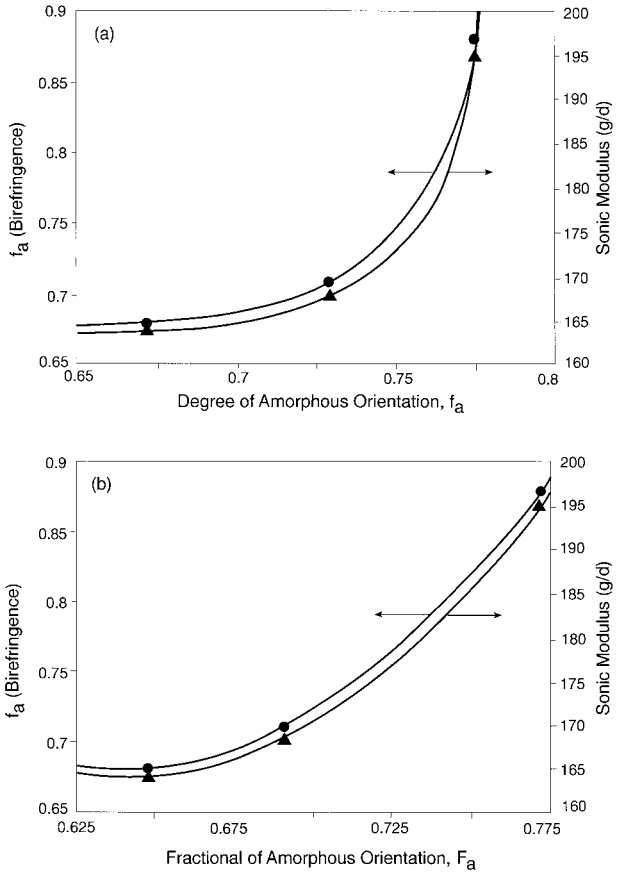

Figure 6 Correlation between XRD amorphous orientation parameters and birefringence and sonic modulus values.

on the conformation of the chains and the interaction between neighboring chains,[19] and hence, on the processing conditions. For instance, Clauss and Salem have shown from a plot of amorphous orientation (obtained from fluorescence measurements) and the birefringence values that Δ_a^o can change from 0.12 for high-speed spun fibers to 0.27 for the spun-drawn fibers.[22] Thus, the "intrinsic" values may not be really "intrinsic," but might depend on the local order in the amorphous and the crystalline regions. Hence, the amorphous orientation determined from birefringence measurements, and by similar reasoning from sonic modulus measurement as well, may not have universal utility.

Orientation and the other characteristics of the crystalline fraction are about the same in all the three fibers. The observed differences in the mechanical properties[7] should therefore be due to other morphological features. Results in Table I and the data in Figure 7 show that amorphous orientation correlates well with tenacity and shrinkage values. The higher shrinkage in 1W70 compared to A330 and 1W90 could be due to the higher fraction anisotropic fraction of the amorphous phase. These segments will tend to become folded just above the glass transition temperature (T_g), and larger this fraction (F_a) and higher the degree of its orientation (f_a), higher will be the shrinkage. Higher amorphous orientation is expected to result in a stiffer chain both below and above T_g. Thus, the shift in the loss tangent maximum to lower temperatures in fiber A330 can be attributed to softer amorphous phase as indicated by its lower amorphous orientation. Data in Figure 7 show that, as with nylon 6,[5] F_a is a more sensitive indicator of orientational distribution of the chain segments in the amorphous phase than f_a, and correlates better with shrinkage and tenacity. On the other hand, it could be that interactions between the crystalline regions and the

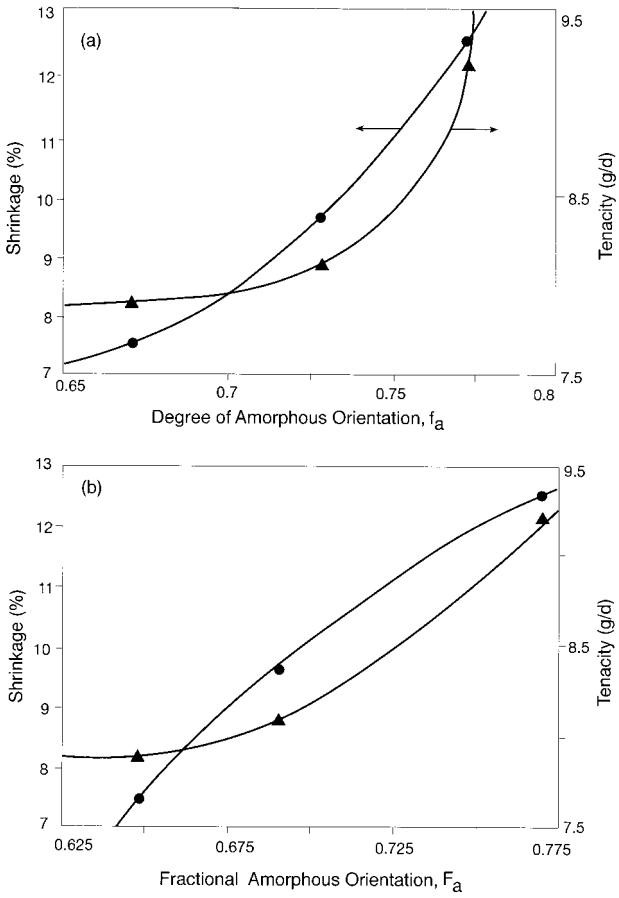

Figure 7 Correlation between XRD amorphous orientation parameters and tenacity and shrinkage data.

amorphous chain segments restrain the amorphous chain segments from shrinking above the T_g. This issue is discussed below.

Although shrinkage and the eventual (high-strain) modulus decrease with decrease in amorphous orientation, the modulus at low strains (<5%) increases with decrease in amorphous orientation. A330 has a higher modulus at low strains and lower modulus at higher strains than the 1W70 fiber. To explain this observation, in addition to the amorphous orientation, we have to consider the linkages or connectivity between the amorphous phase and the crystalline regions. The crystalline regions in A330 appear to act as fillers and account for the high modulus at low strains, retention of the modulus above T_g, and the lower ultimate elongation. Better connectivity between the crystalline and the amorphous regions (both within and outside a fibril) could suppress the yield at low stresses in A330. Lower amorphous orientation could lead to, or be the result of, either or both entanglements within the amorphous regions and the amorphous-crystalline ties. These two factors may restrict the ability of the crystallites to reorient at low strains, and thus increase the modulus at low strains in A330. These entanglements (phantom crosslinks) are not likely to persist at high strains, and the load is borne by the oriented fraction. Hence, the fiber 1W70, which has higher F_a and f_a, has a higher modulus at high strains. These ideas are illustrated schematically in Figure 8(a) and (b), corresponding to the fibers 1W70 and A330, respectively. The Takayanagi models corresponding to these two type of morphology are given in Figure 8(c) and (d). We speculate that 1W70 corresponds to a parallel-series type of arrangement between the amorphous and crystalline regions, where as A330 corresponds to a series-parallel model.[23] Experiments to verify this model are underway.

Enhanced connectivity between the amorphous and the crystalline regions in A330 (the fiber with higher modulus at low strains) would cause this fiber to have higher T_g. Although lower surface energy of the crystals could account for the higher melt temperature in this fiber, this is unlikely because the crystalline parameters, as determined by XRD, are essentially the same in all the fibers. It appears that there is a more efficient transfer of the orientational effects between the amorphous phase to the crystals in A330 than in 1W70. This causes the polymer chains to remain oriented just after melting. The resulting smaller entropy difference between the crystals and the oriented melt at T_m can explain the slightly higher melting point of A330. Similar but more dramatic elevation in melting temperature is observed in gel-spun polyethylene fibers.[24]

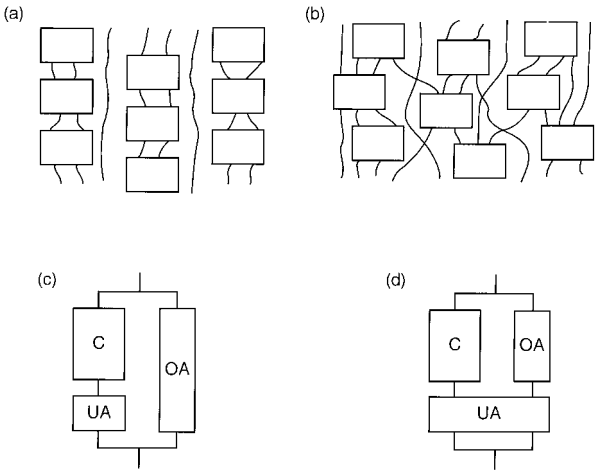

Figure 8 Proposed morphological differences to account for the differences between 1W70 (a) and A330 (b) fibers. Figure b shows the higher degree of crystalline and amorphous linkages, entanglements, and lower amorphous orientation than Figure a. The Takayanagi models corresponding to a and b are shown in c and d, respectively.

CONCLUSIONS

Although lower amorphous orientation (smaller anisotropic fraction) results in fibers with low shrinkage, ties between the crystalline and the amorphous (mostly through unoriented component) regions are important at low strains, and may contribute to increase the glass transition temperature of the fibers. The crystallites acting as fillers account for the higher modulus at low strains and the lower ultimate elongation. The oriented amorphous regions bear the load at higher strains, and the fibers with higher amorphous orientation have higher tenacity.

REFERENCES

1. R. J. Samuels, *Structured Polymer Properties,* Wiley, New York, 1974.

2. G. Jellinek, W. Ringens, and G. Heidemann, *Ber. Bunsenges. Phys. Chem.,* **75,** 924 (1970).
3. P. J. Harget and H. J. Oswald, *J. Polym. Sci., Polym. Phys.,* **17,** 531 (1979).
4. G. W. Urbanczyk, *J. Appl. Polym. Sci.,* **38,** 55 (1989).
5. N. S. Murthy, S. T. Correale, and R. A. F. Moore, *J. Appl. Polym. Sci., Appl. Polym. Symp.,* **47,** 185 (1991).
6. N. S. Murthy, S. T. Correale, and H. Minor, *Macromolecules,* **24,** 1185, (1991).
7. P. B. Rim and C. J. Nelson, *J. Appl. Polym. Sci.,* **42,** 1807 (1991).
8. S. A. Howard, *Adv. X-Ray Anal.,* **32,** 523 (1989).
9. N. S. Murthy and H. Minor, *Polymer,* **31,** 996 (1990).
10. N. S. Murthy, H. Minor, C. Bednarczyk, and S. Krimm, *Macromolecules,* **26,** 1712 (1993).
10. J. E. Fischer, X. Tang, E. M. Scherr, V. B. Cajipe, and A. G. Macdiarmid, *Synthetic Metals,* **41–43,** 661 (1991).
11. Y. Fu, B. Annis, A. Boller, Y. Jin, and B. Wunderlich, *J. Polym. Sci., Polym. Phys.,* **32,** 2289 (1994).
12. Y. Fu, W. R. Busing, Y. Jin, K. A. Affholter, and B. Wunderlich, *Makromol. Chem. Phys.,* **195,** 803 (1994).
13. L. E. Alexander, *X-Ray Diffraction Methods in Polymer Science,* Wiley, New York, 1969.
14. F. J. Balta–Calleja and C. G. Vonk, *X-Ray Scattering of Synthetic Polymers,* Elsevier, Amsterdam, 1989.
15. N. S. Murthy, R. G. Bray, S. T. Correale, and R. A. F. Moore, *Polymer,* **36,** 3863 (1995).
16. J. H. Dumbleton, *Polymer,* **10,** 539 (1969).
17. W. H. Biangardi, *Makromol. Chem.,* **183,** 1785 (1982).
18. A. Wlochowicz, S. Rabiej, and J. Janicki, *J. Appl. Polym. Sci.,* **28,** 1335 (1983).
19. H. J. Biangardi, *J. Polym. Sci., Polym. Phys.,* **18,** 903 (1980).
20. S. K. Garg, *J. Appl. Polym. Sci.,* **27,** 2857 (1982).
21. B. Clauss and D. R. Salem, *Polymer,* **33,** 3193 (1992).
22. I. M. Ward, *Mechanical Properties of Solid Polymer,* Wiley, New York, 1971, pp. 298–314.
24. N. S. Murthy, S. T. Correale, and S. Kavesh, *Polym. Commun.,* **31,** 50 (1990).